Automatic Image Analysis for Processing Marks in Femtosecond Laser Micromachining Using Concave and Convex (unevenness) Coefficient

Daisuke Aoki [1] and Takayuki Tamaki[*1,2]

[1]*Advanced Mechanical Engineering Course, Department of Systems Innovation, Faculty of Advanced Engineering Control Engineering, National Institute of Technology (KOSEN), Nara College, Japan*
[2]*Department of Control Engineering, National Institute of Technology (KOSEN), Nara College, Japan*
[*]*Corresponding author's e-mail: tamaki@ctrl.nara-k.ac.jp*

In this paper, we demonstrate automatic image analysis for processing marks in femtosecond laser micromachining using concave and convex (unevenness) coefficient. To realize laser processing without thermal deformation and cracks, it's important to search optimum processing conditions such as scanning speed and pulse energy. Therefore, we analyzed a set of microscope image during laser microprocessing of glass, and evaluated the morphology such as depth and straightness of processing marks. For the laser microprocessing, an ultrashort laser system (Fianium, FP1060S-PP-D) with a wavelength of 1.06 μm, a pulse duration of 250 fs, and a repetition rate of 1 MHz was used. The sample to be processed was white glass substrates. The sample, which was mounted on the three-dimensional stage, was scanned 10 mm in the *x*-axis direction with a scan speed of 0.1, 0.5, 1, and 2 mm/s. Also, for the laser microprocessing, the pulse energy was changed from 0.9 to 1.3 μJ. After laser microprocessing, processed mark was analyzed with concave and convex coefficient and Otsu's method. By making use of the concave and convex coefficient, luminance unevenness was reduced. We will introduce relationship between "scanning speed and/or pulse energy" and "gray scale and/or straightness of processing marks".
DOI: 10.2961/jlmn.2022.01.2003
Keywords: laser machining, image processing, image analysis, femtosecond laser, optimization, concave and convex coefficient, Otsu's method, unevenness

1. Introduction

In recent years, the joining technology of transparent materials using ultrashort pulsed lasers has attracted much attention [1-3]. The advantages of using ultrashort pulsed lasers to join transparent materials are high strength with minimal thermal deformation, non-contact, no need for a special atmosphere, high speed joining, and the ability to join minute areas. However, the laser welding method uses heat generation due to the linear absorption phenomenon of the medium, which results in melting of the material to be welded over the entire area irradiated by the laser beam [1].

One of the problems in using lasers for joining and machining is the adjustment of machining conditions. Unlike machining with a milling or drilling machine, laser machining requires the adjustment of machining conditions such as laser intensity and focal length. If the machining conditions are not adjusted, heat is generated in excess of the required amount in the case of joining transparent materials using an ultrashort laser pulse, resulting in large thermal deformation. On the other hand, if the amount of heat generated does not reach the required level, problems such as the inability to weld will occur. For this reason, there have been reports on the changes in processing marks when various machining conditions are changed [4-7]. The machining conditions need to be adjusted each time, and the material to be machined is changed. This adjustment is currently performed by the operator who performs the machining based on the rules of experience, so it takes time to adjust the conditions depending on the skill of the operator, and the machining results may vary greatly. It is very difficult to adjust to the optimum conditions, and the current problem is that it relies solely on the experience of the operator. Therefore, there is a need for a computerized system that can make these adjustments mechanically. In fact, a cutting condition setting system has been developed for CO_2 laser cutting machines [8]. However, the accuracy of acoustic emission sensors in this cutting machine varies depending on their dimensions, and this system is based on the data from the acoustic emission sensor. Therefore, in order to construct a general-purpose automatic setting system, we thought of using a camera to photograph the laser processing marks and setting the machining conditions based on the images.

1.1. Observation problem

The current methods for observing the processing marks on a laser-machined part are based on images from a microscope camera or visual observation with the naked eye. Visual observation of processing marks allows us to recognize the exact shape of the marks. Visual observation is mainly used for small-scale machining. For any other processing, observation with the naked eye is not practical. However, it is impossible to extract only the processing marks from the images of processing marks captured by a CCD (Charge

Coupled Device) camera using conventional linear methods of image processing. In this study, it is necessary to extract the area of processing marks on transparent materials in order to analyze the captured images. The reason why the processing marks cannot be extracted by the conventional linear method is that the boundary between the processing marks and the transparent material is ambiguous in the image of laser machining on the transparent material, and the CCD camera generates a specific noise. In addition, when noise reduction is applied, the boundary between the processing marks and the transparent part becomes blurred, and the reduced noise blends into the surrounding pixels, making separation by linear methods even more difficult.

To solve this problem, we introduce the concave and convex (unevenness) coefficient [9] for the images that cannot be binarized by the conventional method. By using the concave and convex coefficient, we can binarize the image without being affected by uneven lighting.

1.2. Study purpose

The purpose of this study is to develop a system to binarize images taken during laser machining using the concave and convex coefficient, and to adjust the machining conditions of the laser based on the binarized images. For this purpose, we will conduct experiments to clarify how the binarized images of the processing marks change when the specific machining conditions are changed. In this experiment, glass was used as the target material, and the surface of the glass was machined in a straight line in a 10 mm. Based on the data obtained from this experiment, we will find the correlation between the machining conditions and the change in the state of the binary image, and our final goal is to develop a system that can automatically set the machining conditions such as laser power and processing speed based on the correlation.

2. Principle of femtosecond laser micromachining

Femtosecond lasers have extremely short pulse widths, ranging from tens to hundreds of femtoseconds, and the light energy is confined in the short pulse widths. The relationship between the pulse train and pulse width of a pulsed laser is shown in Fig.1. In femtosecond lasers, the pulse train is oscillated repeatedly, and the reciprocal of the time interval of the pulse train, i.e., the repetition rate of the light source, is an important factor for laser machining. By focusing the pulse train from such an ultrashort laser inside a transparent material such as glass, it is possible to process the inside of the material locally in a small area near the focal point. In ordinary lasers, the interaction between light and materials is mostly due to linear optics proportional to the electric field. On the other hand, ultrashort pulsed lasers have high peak intensity due to their short pulse widths. Therefore, ultrashort laser pulses are characterized by the contribution of nonlinear optical processes corresponding to the squared and cubed electric fields. In addition, the irradiation of ultrashort laser pulses is terminated before the thermal conduction from electronic to lattice vibrations occurs, thus limiting the heat diffusion area and allowing only a small area to be melted without cracks. When the laser pulse is focused inside the glass, nonlinear absorption phenomena such as multiphoton ionization and tunneling ionization occur in the region near the focus point. This nonlinear absorption causes localized melting of the material and induces a local structural change, thus realizing internal machining.

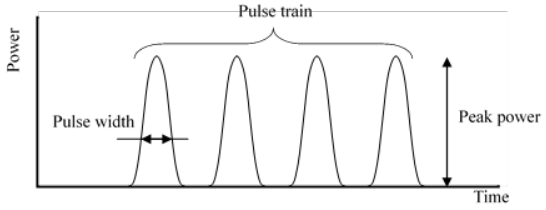

Fig.1 Pulse train and pulse width of pulse laser.

2.1. Feature

A femtosecond laser is a laser with a femtosecond pulse width. In general, laser machining is performed by absorbing laser energy into a material and causing it to melt or evaporate. In this process, the laser-irradiated area needs to be heated above the melting point, which causes thermal effects on the material. The femtosecond laser has a pulse width that is much shorter than the thermal diffusion time of the material, so the thermal effect can be greatly reduced [1].

3. Image processing for extraction of processing marks

3.1. Conventional method(Otsu's binarization method)

Currently, machining is mainly observed visually. In this study, it is necessary to process images of processing marks into images that can be easily analyzed in order to automatically estimate better machining conditions from processing marks. However, the commonly used binarization method may cause problems in the case of images of transparent materials, which are the subject of this study. Here, we explain Otsu's binarization method as one of the common methods.

Otsu's binarization is also called discriminant analysis, and it is a method that automatically performs binarization by finding the maximum threshold value called the degree of separation. The degree of separation can be calculated as the ratio of the inter-class variance to the within-class variance, as follows When the image is binarized with a threshold value *t*, the number of pixels on the side where the luminance value is smaller than the threshold value (black class) is ω_1, the mean is m_1, and the variance is σ_1, the number of pixels on the side where the luminance value is larger (white class) is ω_2, the mean is m_2, and the variance is σ_2, and the number of pixels in the whole image is ω_t, the mean is m_t, and the variance is σ_t. The within-class variance ${\sigma_w}^2$ is

$$ {\sigma_w}^2 = \frac{\omega_1 {\sigma_1}^2 + \omega_2 {\sigma_2}^2}{\omega_1 + \omega_2} $$

The inter-class variance ${\sigma_b}^2$ is

$$ {\sigma_b}^2 = \frac{\omega_1 \omega_2 (m_1 - m_2)^2}{(\omega_1 + \omega_2)^2} $$

The total variance σ_t can be expressed as follows,

$$ {\sigma_t}^2 = {\sigma_b}^2 + {\sigma_w}^2 $$

Therefore, the degree of separation, which is the ratio of the inter-class variance to the within-class variance, can be expressed as

$$ \frac{{\sigma_b}^2}{{\sigma_w}^2} = \frac{{\sigma_b}^2}{{\sigma_t}^2 - {\sigma_b}^2} $$

Here, since the total variance σ_t is constant regardless of the threshold, we can find the threshold t at which the inter-class

variance σ_b^2 is maximized. Furthermore, since the denominator of the inter-class variance formula is also constant regardless of the threshold value.

So, we just need to find the threshold t where the numerator of inter-class variance (σ_b^2) is minimized.

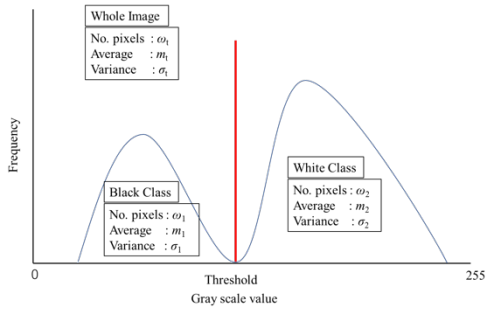

Fig.2 Histogram example.

Otsu's binarization method can binarize an image without any problem if the image has a histogram with a clear boundary between the black and white classes, as shown in Fig. 3. However, since the transparent material in this study transmits light, uneven illumination tends to occur, and the boundary between the material and the processing marks becomes ambiguous. Therefore, when binarization is performed using commonly used binarization methods such as Otsu's method, problems arise in classifying the material, and machining often fails. This is often caused by problems in classifying the image. Fig. 3 shows an example of a failed application of Otsu's binarization method to an actual processing marks image.

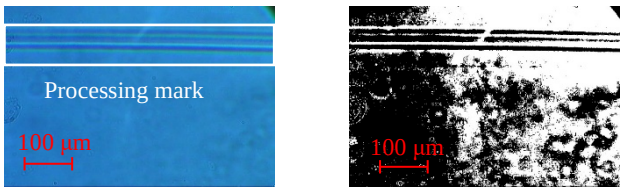

(a) Original image (b) Otsu's method

Fig.3 Failure case in classifying the image.

3.2 Concave and convex coefficient

3.2.1. Calculation of the coefficient

In order to solve the problem of binarization by conventional methods that are commonly used due to the effects of uneven illumination, we use the concave and convex coefficient [9] in this research. By binarizing images using the concave and convex coefficient, binarization can be performed without being affected by uneven lighting. We will now explain how to calculate the concave and convex coefficient.

Fig. 4 shows the calculation range of the smoothing concave and convex coefficient for a 3×3 pixel square, which is the smallest block size. X_{ij} located at the center of the block is the target pixel for calculating the concave and convex coefficient.

$X_{i-1,j-1}$	$X_{i-1,j}$	$X_{i-1,j+1}$
$X_{i,j-1}$	$X_{i,j}$	$X_{i,j+1}$
$X_{i+1,j-1}$	$X_{i+1,j}$	$X_{i+1,j+1}$

Fig.4 Calculation aria of pattern function.

The average luminance value R_{ij} is calculated by constructing a block of a few square pixels on the top, bottom, left, and right sides surrounding X_{ij}. Then, the concave and convex coefficient can be calculated by dividing the target pixel X_{ij} by R_{ij}.

$$\begin{cases} R_{ij} = \dfrac{1}{(2m+1)^2} \displaystyle\sum_{k=-m}^{m} \sum_{l=-m}^{m} X_{i+k,\, j+l} \\ r_{ij} = \dfrac{X_{ij}}{R_{ij}} \end{cases} \quad (1)$$

3.2.2. Characteristics of the coefficient

An example of the frequency distribution of the concave and convex coefficient is shown in Fig. 5.

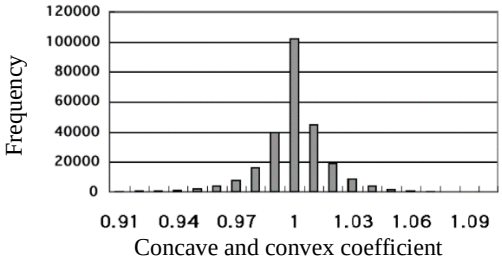

Fig.5 Frequency distribution of pattern function.

The concave and convex coefficient is the concentration of data around 1. Because the image has many flat areas, the correlation between neighboring pixels is strong. From equation (1), 1 is the flat part of the average calculation block. The fact that the value divided by the average luminance value of neighboring pixels is close to 1 means that the luminance value is not significantly different from that of neighboring pixels. On the other hand, if the value divided by the average luminance value of the neighboring pixels is far from 1, it means that there is a large difference between the luminance value and that of the neighboring pixels. This indicates that the part of the target pixel whose value is changing is the part with processing marks. The slope of the luminance of an image can be determined by the concave and convex coefficient.

When the size of the average calculation block is fixed, the concave and convex coefficient of the same pixel shows the same value even if the illumination intensity changes. Because the concave and convex coefficient is calculated based on the average brightness value of the microscopic part of the image, it has no amplitude information. Therefore, the value of the concave and convex coefficient does not change even when the brightness of the illumination changes.

Since the unevenness of illumination changes in a gradual slope, the change in luminance becomes negligible in a

microscopic region such as a block of pixels where the average value of the concave and convex coefficient is calculated.

3.3. Extraction of processing marks

In this paper, we describe the procedure for generating a binary image in which only the processing marks are white from an image in which the processing marks are actually reflected using the concave and convex coefficient.

1) Convert the processing marks image to grayscale.
2) Set the luminance, mean, and standard deviation of the images in 1) to be constant values.
3) Set the concave and convex coefficient calculation range (pixel block size of several square pixels surrounding the pixel) for the pixel of interest $X_{i,j}$ in this study, the block size is set to 17×17).
4) Calculate the concave and convex coefficient r_{ij} from equation (1) to set a good threshold of the image.
5) Binarize an image using the concave and convex coefficient.
6) Use morphological transformations to perform closing and reduce noise.

Fig. 6 shows the result of binarization of Fig. 4 (a) using this machining method.

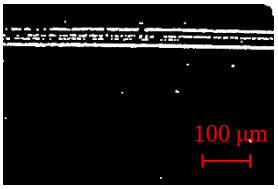

Fig.6 Binary image using adoption method.

4. Processing marks analysis

4.1. Processing marks evaluation

In laser machining, if the machining conditions are not appropriate, the process cannot be carried out properly. Until now, the evaluation of laser processing has been done mainly by visual confirmation. However, in the automatic analysis system for optimal processing marks by computer, which is the objective of this research, it would deviate from the purpose to incorporate the item of visual confirmation into the system. Therefore, it is necessary to propose an evaluation index for processing marks that can be automatically obtained by the computer from images. In this study, we propose the depth of machining and linearity as evaluation indices. The reasons for proposing these two evaluation indices are described below.

Fig. 7 shows three examples of images of processing marks obtained by varying the machining conditions for straight-line surfaces machining of glass.

From Fig. 7(a), it can be seen that when the machining conditions are optimized, the processing marks are straight and darker than the surrounding color. When the laser power is too high or the machining speed is too slow, the processing marks look like Fig. 7(b). In Fig. 7(b), the marks is darker than in Fig. 7(a). On the contrary, Fig.7(c) shows that the machined area is lighter in color than Fig.7(a).

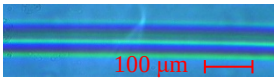

(a) Optimal condition

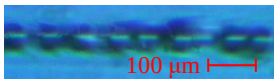

(b) Wrong condition 1

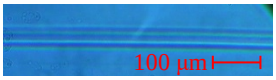

(c) Wrong condition 2

Fig.7 Comparison of processing marks image.

We know from empirical visual observation that the higher the laser power and the slower the machining speed become the deeper machining. From these images, we can see that the deeper marks are darker, and the shallower marks are lighter. This suggests that the depth of machining can be estimated from the grayscale values of the machined parts by converting the images to grayscale. This is one of the proposed evaluation indices.

In addition, among the three images shown in this study, only Fig. 7(b) shows a wobbly processing mark where the lines do not seem to be connected. This indicates that the laser power is too high and the material is subjected to more force than necessary during machining, resulting in cracks. Since cracking during machining is not an appropriate process, it is necessary to evaluate it. Therefore, in addition to the depth of machining described above, we evaluate the linearity of the machined marks. The standard deviation of the width of the line is used to evaluate the linearity of the machined marks. The line width of the machined marks is approximately constant if it is machined in a straight line.

In the case of processing marks such as those shown in Fig. 7(b), the width of the lines varies depending on the location. Therefore, we thought that we could evaluate the linearity by obtaining the width of the line of the machined mark over the entire line and obtaining the standard deviation of the width. If the machining is close to a straight line, the value of the line width is almost constant, i.e., there is little variation in the value, so the value of the standard deviation becomes small. If the machining is wobbly, as in Fig. 7(b), the value of the standard deviation becomes large because the value of the line width has wide fluctuations. These indices are used to evaluate the linearity by computer.

4.2. Image analysis method

4.2.1. Machining depth

As described in Section 4.1, the grayscale value of the image is used to estimate the machining depth. This section describes the machining procedure used in this study.

1) Generate a binary image with only the processing marks extracted using the method described in Section 3.3.
2) Use the binary image in 1) as a mask image and mask the color image of the processing marks image.
3) Perform grayscale transformation on the image generated in 2) (Fig. 8)
4) Calculate the average grayscale value of the image.

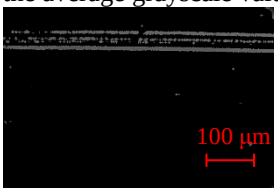

Fig.8 Example of gray scale image for depth estimation.

4.2.2. Linearity

The standard deviation is used to estimate the linearity, and the line widths are acquired as shown in Fig. 9. In Fig. 9, it appears that only four points are acquired, but in fact, the entire line is scanned in the *x*-axis every pixel to acquire the line width data for the entire machining line.

1) Generate a binary image with only the processing marks extracted using the method described in Section 3.3.
2) Get the width of a line from the entire image
3) Calculate the standard deviation of the values in 2)

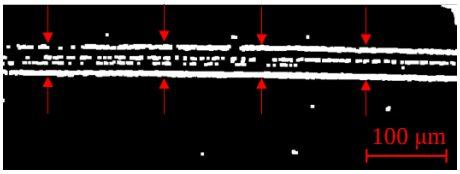

Fig.9 Line width.

5. Experiment

5.1. Experiment setup

The specifications of the femtosecond laser are shown in Table 1.

Table 2 shows the equipment used in the experiment. The optical system is shown in Fig. 10, and (3) and (4) in Table 2 are placed between the polarizer and the half-wave plate to measure the laser power each time after the experiment starts. The plate for fixing the glass is fixed on the automated *XYZ* stage, and then the glass is fixed and installed. The specifications of the femtosecond laser are shown in Table 2.

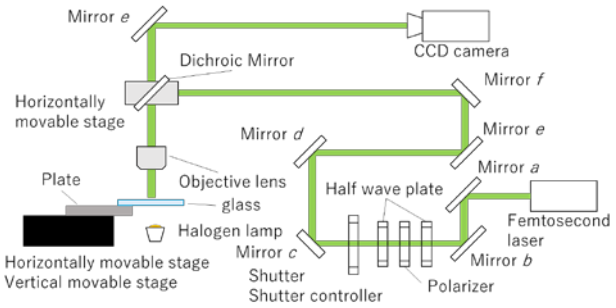

Fig.10 Optical setup.

Table 1 Characteristic of femtosecond laser.

Wavelength [μm]	1.064
Pulse width [fs]	250
Repetition rate [MHz]	1
Maximum power [W]	1.6

Table 2 Experimental equipment and instruments.

	Equipments and Instruments	Manufacturer	Model number
1	Femtosecond laser	Fianium	FP1060S-PP-D
2	Objective lens	OLYMPUS	LMPlan IR (x20/NA0.40)
3	Optical power meter	THORLABS	PM120
4	Sensor head	THORLABS	S310A
5	Shutter	SURUGA SEIKI	F77-4
6	Shutter controller	SURUGA SEIKI	F77-6
7	CCD color camera	SURUGA SEIKI	VCS5270BSET
8	Halogen lamp	FUTABA ELECTRIC	LS-LHA
9	Horizontally movable stage	Newport	XMS100
10	Vertically movable stage	Newport	GTS 30V
11	Capacitive sensor	singletact	S8-10N
12	Camera adapter	TOSHIBA TELI corporation	CA150
13	Glass		B270

5.2. Experimental Procedure

Machining the glass according to the following steps.

1) Prepare a white plate glass (B270) and wipe the surface.
2) Make sure the shutters are closed.
3) Set the femtosecond laser power setting to maximum.
4) Set up a power meter, rotate the half-wave plate, and adjust the laser power to the desired output power (900, 1000, 1100, 1200, 1300 [mW]).
5) Remove the power meter.
6) Mount the glass on the *XYZ* stage.
7) While checking the CCD camera image, adjust the height of the objective lens and the *XYZ* stage so that the image is focused on the glass surface.
8) Open the shutter and confirm that plasma is generated.
9) Close the shutter and move the *XYZ* stage so that it focuses on a clean part of the surface of glass.
10) Set the *x*-direction scanning distance of the *XYZ* stage to 10 mm and the *x*-direction scanning speed to the speed you want to investigate (0.1, 0.5, 1, or 2 [mm/s]).
11) Open the shutter and operate the *XYZ* stage as set in 10).
12) Close the shutter and operate the *XYZ* stage so that the CCD camera shows the starting point of the process.
13) Set the *XYZ* stage scanning speed in the *x*-direction to 1 mm/s, and photograph the processing marks with a CCD camera.
14) Repeat steps from 1) to 13) while changing the laser power and stage scanning speed.

6. Experimental result

6.1 Machining depth

Table 3 and Fig.11 show the changes in the grayscale values when the laser power and machining speed are varied. The experimental results here are the average data of three times each.

Table 3 Depth estimation.

		Laser power [mW]				
		900	1000	1100	1200	1300
		Gray scale value				
Processing speed [mm/s]	0.1	99.74	86.74	65.13	68.02	77.54
	0.5	80.40	94.74	65.70	63.16	81.74
	1	91.99	103.95	78.20	76.05	94.17
	2	102.72	104.09	92.98	84.37	108.53

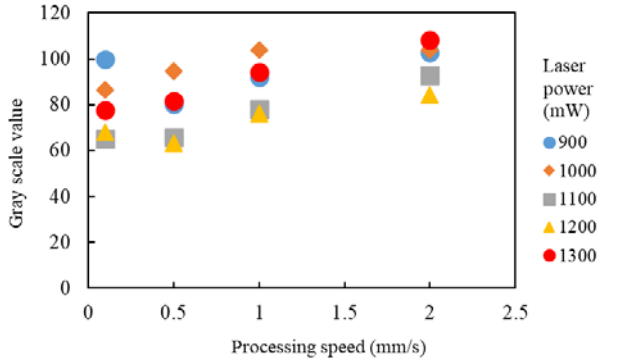

Fig.11 Depth estimation.

Table 3 and Fig.11 show that the higher laser power and slower machining speed tend to be the lower grayscale value. The grayscale value is closer to 0 (black). As mentioned in Section 4.1, the higher laser power and slower machining speed are caused in stronger machining of the material. Therefore, it is considered that the grayscale value can be used to estimate the depth of the processing marks.

6.2. Linearity

Table 4 and Fig. 12 show the change in standard deviation when the laser power and machining speed are changed. The results of each experiment are the average data of three.

Table 4 Evaluation of straightness.

		Laser power [mW]				
		900	1000	1100	1200	1300
		Standard deviation				
Processing speed [mm/s]	0.1	16.82	18.21	18.48	18.19	21.21
	0.5	11.82	7.89	8.98	8.39	9.99
	1	8.62	8.00	13.10	13.44	6.86
	2	7.92	7.85	9.22	10.72	5.00

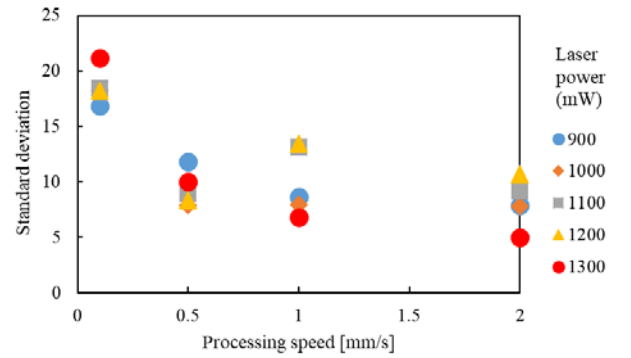

Fig.12 Evaluation of straightness.

Table 4 and Fig. 12 show that the weaker laser power and faster machining speed tend to be smaller standard deviation. The smaller value of standard deviation and the less variation of the value, which means that the straight-line machining can be performed with the same width. On the other hand, a large value of standard deviation means that the variation of values is large, which means that straight line machining cannot be performed with the same width. From the results, it is possible to evaluate whether the machining is normal or not by evaluating the linearity with standard deviation.

7. Discussion

When we look at the experimental data in Chapter 6, we can see that there are some values that deviate slightly from the trend. In order to consider the cause, Fig. 13 shows an image of the processing marks at 900 mW and 0.5 mm/s, which deviates significantly from the trend in the experimental data of machining depth estimation.

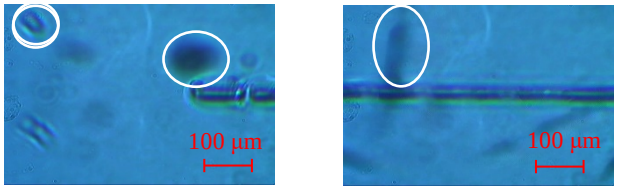

(a) (b)

Fig.13 Error image (900 mW, 0.5 mm/s).

One of the possible causes is that the material is scratched or dusty, as shown in the white ellipses in Fig. 13, or that it is locally blackened as if shaded for some reason. In this study, we use the concave and convex coefficient proposed to obtain a good threshold for shaded images as a binarization method, so if the shadows are caused by uneven lighting in general, the effect can be ignored and binarization can be performed. This method assumes that the shadows are caused by a gradual change in luminance. Therefore, this method cannot completely deal with a sudden change in luminance as shown in Fig. 13(a), and the gray-scale values and standard deviations may be affected to some extent, resulting in abnormal values. Fig. 14 shows a binarized image of Fig. 13(a).

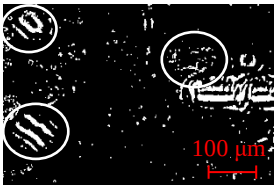

Fig.14 Error binary image.

As you can see, there are still some effects of scratches and dust, and some shadows that cannot be completely erased. These factors affected the grayscale values and standard deviation, resulting in data that deviated from the trend.

In Fig. 13(b), the shadowy area across the processing marks appears to be a little darker than the area without the shadowy area, although the change is not significant. If such objects are more affected by the darker color, it would have a significant impact on the verification of the grayscale value.

As for scratches and dust, the possibility of noise was considered, and therefore, the process to exclude white areas

on the binary image that are far away from the place where processing marks can be recognized in the program was included. The white area in Fig.13 is not a shadow, but the black area is close to the processing mark, and we can assume that the value is far off from the tendency to recognize it as a processing mark and include it in the data. However, since we are basically using only filter image processing in this study, if there are any noises near or on the processing marks, it will be difficult to process all of them with the current machining. If the kernel size is too large, the processing marks themselves will be closed by the closing process and disappear, making further removal difficult. If it is confirmed that the noise is affected by this remaining noise, another noise processing needs to be introduced.

8. Conclusion

In this study, we have been proposed a new binarization method that solves the problem of image processing in transparent materials by using the concave and convex coefficient. We also proposed a direction of quantitative evaluation method to evaluate the machining conditions from the processing marks by using the binary image of the processing marks and analyzing the gray scale values and standard deviation of the processing marks from the image. Until now, laser machining has been mainly evaluated qualitatively by visual inspection or observation with a microscope. If this evaluation method is completed, it is expected that quantitative evaluation of laser machining can be performed.

The amount of data examined in this study is still too small to make a complete estimation. In addition to laser power and machining speed, laser machining is also affected by humidity and temperature, but we have not been able to study these data in this study. Therefore, it is necessary to increase the number of data in the future to obtain more detailed trends of the variation of the processing mark data due to changes in the machining conditions. If we can obtain detailed trends and convert the graphs into mathematical expressions, we can construct a system to estimate machining conditions from processing marks and derive optimal machining conditions. If we can complete this system, we can automate the work of adjusting the machining conditions, which currently depends on the empirical rules of the operator performing the machining, and contribute to the spread of femtosecond laser micromachining.

Reference

[1] W. Watanabe and T. Tamaki: J. Jpn. Soc. Precis. Eng., 81, (2015) 731 (in Japanese).
[2] Y. Kondo, H. Kouta, T. Mitsuyu, and K. Hirao: Oyo Buturi, 69, (2000) 411 (in Japanese).
[3] J. Qiu and K. Hirao: Rev. Laser Eng., 30, (2002) 233 (in Japanese).
[4] Y. Okamoto, T. Sakagawa, H. Nakamura, and Y. Uno: J. Adv. Mech. Des. Syst. Manuf., 2, (2008) 661.
[5] T. Kurita, K. Komatsuzaki, and M. Hattori: Int. J. Mach. Tools Manuf., 48, (2008) 220.
[6] E. Ohmura, M. Kumagai, M. Nakano, K. Kuno, K. Fukumitsu, and H. Morita: J. Adv. Mech. Des. Syst. Manuf., 2, (2008) 540.
[7] A. Assion, T. Baumert, M. Bergt, T. Brixner, B. Kiefer, V. Seyfried, M. Strehle, and G. Gerber: Science 282, (1998) 919.
[8] Y. Konishi, S. Kita, H. Ishigaki, and M. Hasegawa,: Trans. Jpn Soc. Mech. Eng. C, 61, (1995) 299 (in Japanese).
[9] H.Sato and K. Kazuhiro: J. Inst. Image Electron. Eng. Jpn., 36, (2007) 204 (in Japanese).

(Received: June 30, 2021, Accepted: April 11, 2022)